Chall. Nano Micro Scale Sci. Tech., 9(1): 35-47, Winter and Spring 2021
DOI: 10.22111/CNMST.2020.32629.1187

ORIGINAL RESEARCH PAPER

# Three Dimensional Simulation and Performance Enhancement of Evacuated U–Tube Solar Collectors Filled with Nanofluid

***Hossein Pourmohamadian****

*Department of Mechanical Engineering, Naragh Branch, Islamic Azad University, Naragh, Iran*

*Received 4 March 2020; revised 28 October 2020; accepted 22 November 2020 available online 2 September 2021*

**ABSTRACT:** In this paper, forced convection flow and heat transfer of Cu-water nanofluid in U-Tube collector are studied. The three-dimensional governing equations are numerically solved in the domain by the control volume approach based on the SIMPLE algorithm. Reynolds numbers are considered in laminar-turbulent range of 2000<Re<8000. The most efficient model was achieved by comparison of different parameters to reach the optimal case with the maximum exergy efficiency. From this study, it is concluded that in the case of using U-tube, instead of shell and tubes, the time that the fluid is inside the collector increases and leads to outlet temperature increase from the collector the exergy efficiency increases. Also, it is realized that enhance the outlet fluid temperature, energy efficiency and exergy efficiency. Generally, while the trend of exergy efficiency variation with effective parameters is increasing, applying the mixers precipitate the efficiency increment. In addition, for the case that the trend of exergy efficiency variation with changing these parameters is decreasing, the decreasing trend gets slow. The exergy efficiency of studied UTC at 14:00 has the maximum exergy efficiency among all studied times and about 71.54%. The received energy always reduces by increasing of operating temperature. The value of received energy at operating temperature of 23°C is about 0.347 kW/m$^2$. The nanofluid flow has higher thermal conductivity than the base fluid and can absorb more solar irradiances. But the nanofluid has also more dynamic viscosity than base fluid which increases the pressure drop penalty and friction factor in system. Finally, the highest exergy efficiency was obtained for the nanoparticle volume fraction of $\phi$=4%. Therefore, the UTC with tube diameter of 8nm filled with Cu-water nanofluid with 4% volume fraction and 40nm nanoparticle diameter at Re=2000 is introduced as the best model in present study.

**KEYWORDS:** *U-tube collector, Exergy efficiency, Radiation, Forced convection, Nanofluid*

## INTRODUCTION

As a clean and renewable energy source, solar energy has good prospects for solving energy and environmental problems in the future. The concentrated U-Tube collector (UTC) systems are a popular way to generate semi-high-temperature heat source by absorbing and converting solar energy into heat energy. This system possesses the most commercialized markets and mature technology, and it is widely applied in semi-high-temperature solar thermal fields, such as solar cooling, solar desalination, and concentrated solar power (CSP) generation [1-8]. A lot of research work has been carried out to study the use of UTCs in solar thermal field.

Kaya et al. [1] experimentally investigated thermal performance of an evacuated U-Tube solar collector with ZnO/Etylene glycol-pure water nanofluids. Naik and Muthukumar [2] in a numerical study investigated performance assessment of evacuated U-tube solar collector. They found that employing water and air as copper, aluminum and brass as U-tube material, and graphite, magnesium oxide and aluminum oxide as filler material and the performance of the evacuated tube solar collector is investigated in detail. Kaya and Arslan [3] numerically investigated efficiency and economic analysis of an evacuated U-tube solar collector with different nanofluids.

Their findings reveal that the using of solar energy comprehensively is more beneficial for health of earth. Sadeghi et al. [4] investigated experimentally and numerically performance of evacuated tube solar collectors, applying synthesized $Cu_2O$/distilled water nanofluid. They found that usage of nanofluid has a significant effect on thermal-hydraulic efficiency of system. Wang et al. [5] examined the idea of using a radiation shield in the upper part of the absorber tube. This part aims to reduce the thermal losses of the PTC. Yang et al. [6] proposed a double coating solar collector which uses different coatings in the upper and in the down part of the absorber. Based on their obtained results, usage of coatings can enhance thermal efficiency of system.

*Corresponding Author Email: *hosseinpm@yahoo.com*
Tel.: +989133613133; Note. This manuscript was submitted on March 4, 2020; approved on October 28; published online September 2, 2021.

Naphon and Kornkumjayrit [7] conducted a numerical investigation inside one-sided corrugated plate in turbulent flow regime. He found that used geometry has significant effect on heat transfer process. In another numerical study by Naphon [8], he conducted a study on the effect of wavy plate geometry on fluid flow and heat transfer of air in turbulent flow regime. Their results shown an increased in heat transfer and pressure drop. A numerical study on turbulent flow by Assato and de Lemos [9] in periodically sinusoidal-wavy channels was done. A numerical study on wavy wall micro-channels having rectangular cross section was done by Sui et al. [10]. Their results showed that usage of wavy wall channel can enhance the heat transfer and increase the pumping power. Duan and Muzychka [11] presented an analytical study for laminar flow regime on the axial corrugated surface roughness effect on flow field and heat transfer inside micro-tubes. They observed an increase in required pumping power (pressure drop). A numerical investigation on corrugation profile for cross-corrugated plates effect on flow field and heat transfer were conducted by Zhang and Che [12]. Reported results showed that trapezoidal channel has higher Nusselt number and friction factor than the elliptic channel. In another work Zhang and Che [13] carried out a three-dimensional numerical investigation presenting an analysis on Nusselt number and friction factor. As can be seen from above research studies, all of the cited work on conventional fluids in wavy channels had better heat transfer (or Nusselt number) and greater pressure drop (required pumping power) compared with results of straight channel. The annual irradiation on the collector plane is improved by introducing corrugated booster reflectors instead of flat booster reflectors [14]. The optimum inclination of the collector and flat plate booster reflector is reported theoretically to augment the performance of the solar collector [15]. Monowe et al. [16] planned a portable single basin solar still with an external reflecting booster and an outside condenser. They determined that the loss of latent heat of condensation to the environment had been minimized. The optimum position of flat plate booster reflectors is examined by Kostic and Pavlovic [17] on thermal performance of the solar collector. They found that usage of turbulators and employing of nanofluids has a significant effect on thermal-hydraulic efficiency of system. Kostic and Pavlovic [18] also studied the effect of four aluminum flat plate reflectors which were placed in the bottom, top, right and left side of the solar collector during day time over the year. Hiroshi [19] numerically investigated the improvement in absorbed solar radiation of a flat plate solar thermal collector by a flat plate bottom reflector.

The literature review elucidates that although the effect of U-Tube solar collectors on heat transfer has been assessed (see Refs. [20-28]), but the effects of using nanofluid on energy and exergy efficiency in U-Tube solar collectors based on present experimental data have not been yet investigated numerically. The coating is vacuum and the fluid flow is in turbulent regime. Using the results of this paper the researchers attain a new method to analyze the energy efficiency of vacuumed U-Tube solar collectors numerically. In present study using 3D simulation the performance enhancement of evacuated U–Tube solar collectors filled with nanofluid is investigated. The main application is in solar energy field, where usage of solar collectors with higher energy efficiency has nowadays attracted a lot of attention. Also it is expected that usage of U-Tube systems can also enhance the energy efficiency of concentrated collectors.

## NUMERICAL MODEL

### Physical Model

The schematic diagram of studied U-Tube solar collector is shown in Fig. 1. Table 1 represents different properties of this collector. The reason of this selection is the empirical data available for validation and compression. For simulation, useful received energy by collector is calculated based on inlet solar radiation and overall heat loss using analytical relations. In the following, the collector simulated numerically and useful received energy by fluid, outlet temperature of fluid, Nusselt number and energy- and exergy efficiency are calculated. The flow inside the channel is considered at steady state condition and turbulent flow regime. Velocity inlet and pressure outlet conditions are assumed for the inlet and the outlet section of the collector. Referred collector is under the uniform heat flux that is calculated using optical properties and overall heat loss of collector for different months based on empirical measurements results of Sabziparvar [29].

### Numerical Method

The system of governing equations for fluid flow and heat transfer in the flat–plate sheet and tube solar collector can be written in the Cartesian tensor system as [30]:

$$\frac{\partial}{\partial x_i}(\rho u_i) = 0 \tag{1}$$

$$\frac{\partial}{\partial x_j}(\rho u_i u_j) = -\frac{\partial P}{\partial x_i} + \frac{\partial}{\partial x_j}\left[\mu\left(\frac{\partial u_i}{\partial x_j} + \frac{\partial u_j}{\partial x_i}\right)\right] + \frac{\partial}{\partial x_j}\left(-\rho\overline{u_i' u_j'}\right) \tag{2}$$

$$\frac{\partial}{\partial x_i}(\rho u_i T) = \frac{\partial}{\partial x_j}\left[(\Gamma + \Gamma_t)\frac{\partial T}{\partial x_j}\right] \tag{3}$$

where $\rho$ is the fluid density and $u_i$ is the axial velocity, $\mu$, $\acute{u}$ and $u_j$ are the fluid viscosity, fluctuated velocity and

the axial velocity, respectively, and the term $-\rho\overline{u_i'u_j'}$ is the turbulent shear stress.

With using the Reynolds averaged approach for modeling the flow field and heat transfer in turbulence flow regime, it is requires to model the Reynolds stresses $-\rho\overline{u_i'u_j'}$ in Eq. (2). For closure of the equations, the $k$–$\varepsilon$ turbulence model was chosen. A common method employs the Boussinesq hypothesis to relate the Reynolds stresses to the mean velocity gradient as [30-37]:

$$\left(-\rho\overline{u_i'u_j'}\right) = \mu_t\left(\frac{\partial u_i}{\partial x_j} + \frac{\partial u_j}{\partial x_i}\right) \tag{4}$$

The turbulent viscosity term $\mu_t$ is to be calculated using an appropriate turbulence model. The turbulent viscosity expression is given as [30]:

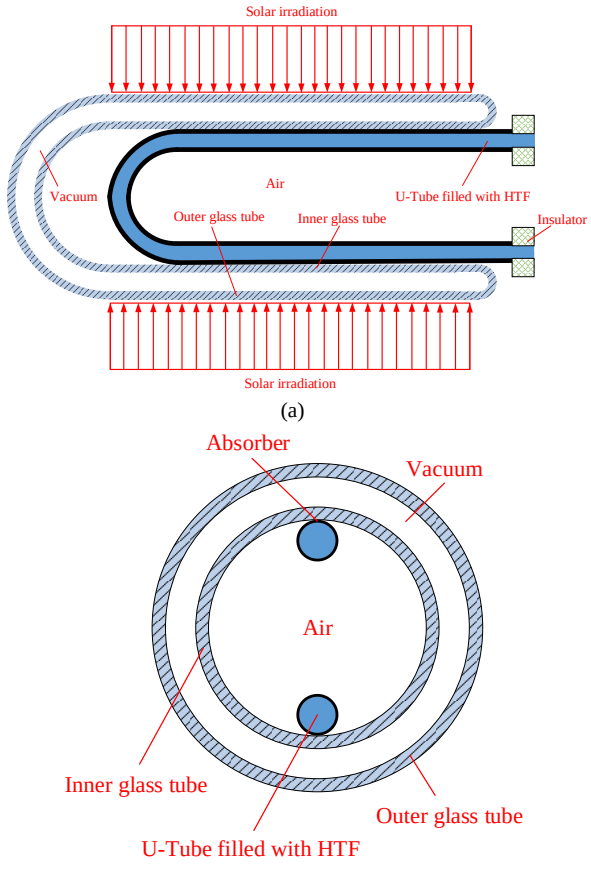


**Fig.1.** Schematic diagram of U-Tube solar collector: **a)** Front view **b)** Side view

$$\mu_t = \rho C_\mu \frac{k^2}{\varepsilon} \tag{5}$$

Where $k$, is turbulence kinetic energy (TKE) and calculated from the following equation [30]:

$$\frac{\partial}{\partial x_i}[\rho k u_i] = \frac{\partial}{\partial x_j}\left[\left(\mu + \frac{\mu_t}{\sigma_k}\right)\frac{\partial k}{\partial x_j}\right] + G_k - \rho\varepsilon \tag{6}$$

Similarly, in the TKE dissipation rate, ε is written by the following equation [30]:

$$\frac{\partial}{\partial x_i}[\rho\varepsilon u_i] = \frac{\partial}{\partial x_j}\left[\left(\mu + \frac{\mu_t}{\sigma_\varepsilon}\right)\frac{\partial \varepsilon}{\partial x_j}\right] + C_{1\varepsilon}\frac{\varepsilon}{k}G_k + C_{2\varepsilon}\rho\frac{\varepsilon^2}{k} \tag{7}$$

where $G_k$ is the generation rate of the TKE and $\rho\varepsilon$ is its destruction rate. $G_k$ is calculated as follow [25]:

$$G_k = -\rho\overline{u_i'u_j'}\frac{\partial u_j}{\partial x_i} \tag{8}$$

**Table 1**
The specifications of the studied collector [20]

| Specification | Value / Detail | Unit |
|---|---|---|
| Occupied area | 200×94×9.5 | cm |
| Absorption area | 1.51 | $m^2$ |
| Weight | 38.5 | kg |
| Frame | Aluminum 6063 | |
| Glass (Float) | $t$ = 4 | mm |
| Emissivity of glass covers | 0.85 | – |
| Quantities of glass covers | One | – |
| Header pipe (Cu) | Ø22, $t$ = 0.9 | mm |
| Connector riser to absorber (Cu) | Ø10, $t$ = 0.9 | mm |
| Thermal emission of absorber | 7 | % |
| Thermal conductivity of absorber | 211 | $W{\cdot}m^{-1}{\cdot}K^{-1}$ |
| Thickness of plate | 2 | mm |
| Slop of collector | 45 | degree |
| Solar absorption | 96.2 | % |
| Coating method | Vacuum | – |
| Thermal conductivity of insulators | 0.05 | $W{\cdot}m^{-1}{\cdot}K^{-1}$ |
| Thickness of insulators | 20 | mm |
| Optical efficiency | 68 | % |

The enhanced wall treatment method is chosen to assume turbulent quantities through pipes. The empirical constants including $C_\mu$=0.09, $C_{1\varepsilon}$=1.44, $C_{2\varepsilon}$=1.92, $\sigma_k$=1.00, $\sigma_\varepsilon$=1.30 and $Pr_t$=0.90 are chosen in the turbulence transport equations [30]. Bellow assumptions are determined:

- The problem is steady state.

- The flow regime is turbulent.
- The fluid flow is incompressible.
- The nanofluid has Newtonian behavior.
- The nanofluid is single phase.
- Diffuse solar irradiations are not absorbed.

The fluid is considered to be Newtonian, and the physical properties of the fluid are temperature dependent. Since the temperature variation is higher than 3°C [31], the following polynomial expressions are used [32]:

$$\rho(T) = 5.37380 \cdot 10^{-10}T^5 - 9.59976 \cdot 10^{-7}T^4 + 6.93809 \cdot 10^{-4}T^3 - 0.255822T^2 + 47.8074T - 2584.53 \quad (9)$$

$$c_p(T) = -4.51782 \cdot 10^{-8}T^5 + 7.61613 \cdot 10^{-5}T^4 - 5.12699 \cdot 10^{-2}T^3 + 17.2363T^3 - 2894.85T + 198532 \quad (10)$$

$$k(T) = 5.15307 \cdot 10^{-11}T^5 - 8.15212 \cdot 10^{-8}T^4 + 5.1380 \cdot 10^{-5}T^3 - 1.61344 \cdot 10^{-2}T^2 + 2.52691T - 157.532 \quad (11)$$

$$\mu(T) = -4.37087 \cdot 10^{-13}T^5 + 7.38482 \cdot 10^{-10}T^4 - 4.99292 \cdot 10^{-7}T^3 + 1.68946 \cdot 10^{-4}T^2 - 2.86313 \cdot 10^{-2}T + 1.94641 \quad (12)$$

For closing the system of governing equations, a set of boundary condition is required. Velocity inlet for inlet, pressure outlet for outlet and non-slip with constant heat transfer between the fluid and side for side of pipes were applied.

The spectral radiative transfer equation (RTE) can be written as [30-32]:

$$\frac{dI_v(r,s)}{ds} = -(K_{av} + K_{sv})I_v(r,s) + K_{av}I_b(v,T) + \frac{K_{sv}}{4\pi}\int_{4\pi} dI_v(r,s') \cdot \phi(s,s')d\Omega' + S \quad (13)$$

where $I_v$ is spectral radiation intensity which depends on position r and direction s [30-32]:

$$I_v(r,s) = \varepsilon_v(r_w)I_b(v,T) + \frac{\rho_w(r_w)}{\pi}\int_{n\cdot s'<0} I_v(r,s') \cdot |n \cdot s'|d\Omega' \quad (14)$$

The commercial ANSYS-FLUENT was used to solve the governing equations. The control volume approach was used to solve the system of classical single phase governing equations by using the finite volume method. The standard *k–ε* turbulence model with enhanced wall function was selected. The diffusion term in the momentum and energy equations was approximated by second-order central difference. In addition, a second–order upwind differencing scheme was adopted for the convective terms. The convergence criterion was considered $10^{-6}$ for all variables.

## Analytical Method

Useful received energy by fluid in collector is calculated as follow [33]:

$$\dot{Q}_{u,f} = \dot{m}_f c_p(T_{out} - T_{in}) \quad (15)$$

where $\dot{m}_f$ is working fluid mass flow rate of, $c_p$ is fluid constant specific heat capacity and $T_{in}$ and $T_{out}$ are mean fluid inlet and outlet temperature, respectively.

Useful received energy by collector based on inlet solar radiation and overall heat loss is as follow [33]:

$$\dot{Q}_{u,c} = A_c\left(S - U_L\left(T_{pm} - T_a\right)\right) \quad (16)$$

Where $A_c$ is the area of absorber plate, $T_a$ is ambient temperature and $T_{pm}$ is mean temperature of plate. In the present study temperature gradients around the pipe can be neglected and a mean temperature can be taken into account for it as far as pipe has been spread through the plate, and also the thermal conductivity of bond part, thermal conductivity of plate and the convection heat transfer coefficient of fluid are high. Also *S* is a part of solar radiation per plate area unit that is absorbed by plate and is as [33]:

$$S = \eta_0 \cdot I_T \quad (17)$$

where $I_T$ is daily average hourly radiation entered to collector and $\eta_0$ is optical efficiency of collector and is calculated as follow [33]:

$$\eta_0 = (\tau\alpha) = 1.01\tau\alpha \quad (18)$$

where $\tau$ and $\alpha$ refer to solar transmission and solar absorption coefficient. Also, $I_T$ is calculated as [28]:

$$I_T = I_b R_b + I_d\left(\frac{1+\cos\beta}{2}\right) + I \cdot \rho_{gr}\left(\frac{1-\cos\beta}{2}\right) \quad (19)$$

where *I*, $I_b$ and $I_d$ are solar radiation on horizontal surface, beam radiation and diffuse radiation, respectively.

Also, $R_b$ is ratio of beam radiation on tilted surface to that on horizontal surface and is calculated as follow [33]:

$$R_b = \frac{\cos(\varphi-\beta)\cos\delta\cos\omega+\sin(\varphi-\beta)\sin\delta}{\cos\varphi\cos\delta\cos\omega+\sin\varphi\sin\delta} \quad (20)$$

where $\varphi$ is latitude of collector location, $\delta$ is declination angle and $\omega$ is hour angle. Furthermore, $U_L$ in Equation (5) is collector overall heat loss coefficient and is calculated as follow [33]:

$$U_L = U_t + U_b + U_e \quad (21)$$

where $U_t$ is top loss coefficient, $U_b$ is back loss coefficient and $U_e$ is edge loss coefficient. The top loss coefficient is calculated as follow [33]:

$$U_t = \left(\frac{N}{\frac{C}{T_{pm}}\left[\frac{T_{pm}-T_a}{N+f}\right]^e}+\frac{1}{h_w}\right)^{-1} + \frac{\sigma\left(T_{pm}+T_a\right)\left({T_{pm}}^2+{T_a}^2\right)}{\frac{1}{\varepsilon_p+0.0059N\cdot h_w}+\frac{2N+f-1+0.133\varepsilon_P}{\varepsilon_g}} \quad (22)$$

$$f = \left(1+0.089h_w-0.1166h_w\varepsilon_p\right)(1+0.07866N) \quad (23)$$

$$C = 520(1-0.000051\beta^2) \quad (24)$$

$$e = 0.430\left(1-\frac{100}{T_{pm}}\right) \quad (25)$$

$$h_w = 2.8+3V_w \quad (26)$$

Where $N$ is number of glass covers, $h_w$ is wind heat transfer coefficient, $V_w$ is wind velocity and $\sigma$ is Stefan Boltzmann constant. Also the back loss coefficient is defined as follow [33]:

$$U_b = \frac{k}{L} \quad (27)$$

In order to analyze and compare the fluid flow characteristics and heat transfer of different suspended nanoparticles volume fractions and different nanoparticle shapes in collector, some definitions are given as follows. Fluid Reynolds number is defined as [30-37]:

$$\mathrm{Re} = \frac{\rho_f\cdot u_m\cdot D_i}{\mu_f} \quad (28)$$

where $u_m$ referred to the fluid mean velocity over the cross section. The Nusselt number is defined as [30]:

$$\mathrm{Nu} = \frac{h_f\cdot D_i}{k_f} \quad (29)$$

where $h_f$ and $k_f$ represent the heat transfer coefficient and the fluid thermal conductivity, respectively.

The pressure drop between inlet and outlet is defined as [30]:

$$\Delta P = P_{av,inlet} - P_{av,outlet} \quad (30)$$

The friction factor for fully developed flow is expressed as follows [30]:

$$f = \frac{2}{\left(\frac{L}{D_i}\right)}\frac{\Delta P}{\rho_{nf}\cdot {u_m}^2} \quad (31)$$

Total entropy generation, $\dot{S}_{gen}$ (W/K), in the collector can be obtained via the amount of lost work, $\dot{W}_{lost}$, that is the summation of leakage ($\dot{E}_l$) and destroyed ($\dot{E}_d$) exergy rates. The total entropy generation rate can be expressed as [20]:

$$\dot{S}_{gen} = \frac{\dot{W}_{lost}}{T_a} + \frac{\dot{E}_d+\dot{E}_l}{T_a} \quad (32)$$

The destroyed exergy rate can be obtained by the following relation [20]:

$$\dot{E}_d = \dot{E}_{d,\Delta T_s} + \dot{E}_{d,\Delta P} + \dot{E}_{d,\Delta T_f} \quad (33)$$

where $\dot{E}_{d,\Delta Ts}$ is the destroyed exergy rate due to the temperature difference between sun and absorber plate and written as follow:

$$\dot{E}_{d,\Delta T_s} = \eta_0 G_t A_C T_a\left(\frac{1}{T_p}-\frac{1}{T_S}\right) \quad (34)$$

$\dot{E}_{d,\Delta P}$ is the destroyed exergy rate due to pressure drop in the collector and calculated as:

$$\dot{E}_{d,\Delta P} = \frac{\dot{m}\Delta P}{\rho}\cdot\frac{T_a\ln\left(\frac{T_{out}}{T_a}\right)}{T_{out}-T_{in}} \quad (35)$$

Also $\dot{E}_{d,\Delta Tf}$ is the destroyed exergy rate due to the flow of nanofluid in the collector and the temperature difference between nanofluid and absorber plate and obtained as follow:

$$\dot{E}_{d,\Delta T_f} = \dot{m}c_pT_a\left(\ln\left(\frac{T_{out}}{T_a}\right)-\frac{T_{out}-T_{in}}{T_P}\right) \quad (36)$$

The leakage exergy rate is:

$$\dot{E}_l = U_l A_c (T_P - T_a)\left(1 - \frac{T_a}{T_P}\right) \tag{37}$$

Therefore the developed form of Eq. (30) can be written as following equation:

$$\dot{S}_{gen} = \underbrace{\eta_0 G_t A_c \left(\frac{1}{T_p} - \frac{1}{T_S}\right) + \dot{m} c_p \left(\ln\left(\frac{T_{out}}{T_{in}}\right) - \frac{T_{out} - T_{in}}{T_P}\right) + U_l A_c \left(\frac{T_P}{T_a} - 1\right)\left(1 - \frac{T_a}{T_P}\right)}_{\dot{S}_{gen,H}} + \underbrace{\frac{\dot{m}\Delta P}{\rho} \cdot \frac{T_a \ln\left(\frac{T_{out}}{T_a}\right)}{T_{out} - T_{in}}}_{\dot{S}_{gen,F}} \tag{38}$$

where $\dot{m}$ is the total mass flow rate of nanofluid (kg/s), $\Delta P$ is pressure drop (Pa), and $T_S$ is apparent sun temperature. As shown in Eq. (34), the entropy in the solar collector is generated by two effects, first the temperature gradients and consequently heat transfer, $\dot{S}_{gen,H}$, and the second is velocity gradients that lead to fluid friction and pressure drop, $\dot{S}_{gen,F}$. To calculate the nanofluid thermophysical properties, following equations are proposed [30]:

$$\rho_{nf} = (1-\phi)\rho_f + \phi\rho_{np} \tag{39}$$

$$(C_P)_{nf} = \frac{(1-\phi)(\rho C_P)_f + \phi(\rho C_P)_{np}}{\rho_{nf}} \tag{40}$$

$$\frac{k_{nf}}{k_f} = 1 + 4.4\, Re_p^{0.4}\, Pr_f^{0.66} \left(\frac{T}{T_{fr}}\right)^{10} \left(\frac{k_p}{k_f}\right)^{0.03} \phi^{0.66} \tag{41}$$

$$Re_{np} = \frac{2\rho_f k_b T}{\pi {\mu_f}^2 d_p} \tag{42}$$

In this model, $Re_p$ is the nanoparticle Reynolds number, Pr is the Prandtl number of the base liquid, $T$ is the nanofluid temperature, $T_{fr}$ is the freezing point of the base liquid, $k_p$ is the nanoparticle thermal conductivity, and $\phi$ is the volume fraction of the suspended nanoparticles. Also, $\rho_f$ and $\mu_f$ are the mass density and the dynamic viscosity of the base fluid, respectively, and $d_p$ and $u_B$ are the nanoparticle diameter and mean Brownian velocity, respectively. Assuming absence of agglomeration, the nanoparticle Brownian velocity $u_B$ is calculated as the ratio between $d_{np}$ and the time $\tau_D$ required to cover such distance. Also, thermophysical properties of water and Cu are reported in Table 2.

**Table 2**

Thermophysical properties of water and Cu are reported

| Material | $\rho\left(\frac{Kg}{m^3}\right)$ | $k\left(\frac{W}{m.K}\right)$ | $c_p\left(\frac{J}{Kg.K}\right)$ | $\mu\left(\frac{Ns}{m^2}\right)$ |
|---|---|---|---|---|
| Water | 998.2 | 0.6 | 4182 | 0.001003 |
| Cu | 8993.0 | 385.0 | 400 | - |

## Validation

As shown in Table 3 a grid independence test was performed for the collector to analyze the effects of grid sizes on the results. As it is seen six sets of mesh are generated and tested. By comparing the results, it is concluded that mesh configurations contains grid number of 1,924,313 nodes has been adopted to get an acceptable compromise between the computational time and the result accuracy with an error of 0.03 percent. Also the computer code validation was done by comparison of numerical results obtained from present study and results of Gupta and Saha [38] at same geometrical dimension and boundary condition. Fig. 2 shows these results compression. As can be seen from Fig. 2 remarkable agreement exists between the data [38] and numerical results obtained from present study with maximum error of ±0.4 K.

**Table 3**

Grid independence test for studied collector

| No. | Nodes | $T_{out}$ (°C) | Error (%) |
|---|---|---|---|
| 1 | 462,727 | 84.4579 | 15.51 |
| 2 | 856,009 | 71.3579 | 6.27 |
| 3 | 1,293,58 | 66.8734 | 9.27 |
| 4 | 1,555,552 | 60.6703 | 3.96 |
| 5 | 1,744,623 | 58.2745 | 0.03 |
| 6 | 1,924,313 | 58.2567 | – |

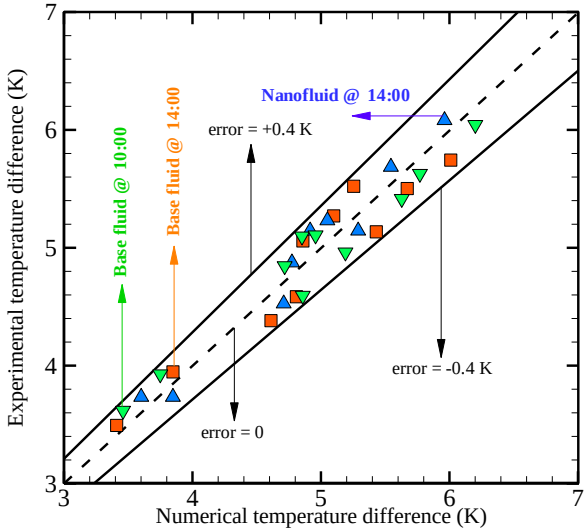


**Fig. 2.** Code validation for outlet temperature based on experimental data [38] for water as working fluid

## RESULT AND DISCUSSION

In this section, firstly the energy and exergy efficiencies of UTC filled with base fluid and nanofluid are compared. Table 4 shows energy and exergy efficiencies of the studied UTC filled with water during different hours of day and also Table 5 illustrates energy and exergy efficiencies for UTC filled with nanofluid during different hours of day. As it is seen:

- The values of absorber temperature in case of using nanofluid are amore than case of using base fluid.
- The values of energy loss in case of using nanofluid are amore than base fluid. This behavior is because of more temperature of absorber plate in nanofluid case.
- The values of outlet flow temperature in case of using nanofluid are less than base fluid. This behavior is because of more heat loss in nanofluid case.
- Energy and exergy efficiencies of nanofluid cases are more than base fluid ones during all studied hours.

Fig. 3 shows effects of using nanofluid on different parameters of studied UTC. Fig. 3a shows effects of different solar intensity on received energy of studied UTC filled with nanofluid. The nanofluid flow has higher thermal conductivity than the base fluid and can absorb more solar irradiances. But the nanofluid has also more dynamic viscosity than base fluid which increases the pressure drop penalty and friction factor in system. As it is seen in this figure, the received energy always increases by increasing of solar intensity.

**Table 4**
Energy and exergy efficiencies for UTC filled with base fluid

| Time | $I_T$ (W/m$^2$) | $U_L$ (W/m$^2$·K) | $T_{pm}$ (°C) | $T_{out}$ (°C) | $\eta$ (%) | $\psi$ (%) |
|---|---|---|---|---|---|---|
| 09:00 | 560 | 7.33 | 48.11 | 58.59 | 54.29 | 3.34 |
| 09:30 | 630 | 7.37 | 49.06 | 59.61 | 57.48 | 3.53 |
| 10:00 | 750 | 7.32 | 51.32 | 61.04 | 57.78 | 3.95 |
| 10:30 | 830 | 7.49 | 52.41 | 62.61 | 64.40 | 4.21 |
| 11:00 | 925 | 7.56 | 54.25 | 65.82 | 63.00 | 4.35 |
| 11:30 | 992 | 7.52 | 57.07 | 67.07 | 63.68 | 4.58 |
| 12:00 | 1006 | 7.56 | 58.42 | 69.23 | 61.91 | 4.60 |
| 12:30 | 1020 | 7.77 | 59.31 | 70.26 | 61.54 | 4.55 |
| 13:00 | 978 | 7.76 | 60.46 | 72.04 | 61.48 | 4.54 |
| 13:30 | 914 | 7.40 | 60.57 | 72.61 | 60.16 | 4.68 |
| 14:00 | 834 | 7.73 | 63.22 | 75.13 | 58.64 | 4.67 |
| 14:30 | 780 | 7.55 | 63.47 | 75.77 | 57.57 | 4.56 |
| 15:00 | 734 | 7.77 | 63.89 | 76.41 | 56.91 | 4.41 |
| 15:30 | 626 | 7.94 | 64.09 | 76.91 | 56.28 | 4.21 |
| 16:00 | 607 | 7.97 | 65.11 | 77.82 | 55.62 | 4.15 |

The value of received energy at solar intensity of 0.88 W/m$^2$ is about 0.331 kW/m$^2$. Fig. 3b shows effects of different flow rates on received energy of studied UTC filled with nanofluid. As it is seen in this figure, the received energy always increases by increasing of flow rate. The heat transfer rate always increases by mass flow rate. Higher flow velocities lead to more turbulent flow and more vortex generation in system which increases flow mixing rate in channel. This leads to more heat transfer coefficient and increases the heat transfer rate in system. The value of received energy at flow rate value of 24 mL/s is about 0.472 kW/m$^2$. Fig. 3c shows effects of different inlet flow temperature on received energy of studied UTC filled with nanofluid. As it is seen in this figure, the received energy always increases by increasing of inlet flow temperature. The value of received energy at inlet flow temperature of 31°C is about 0.169 kW/m$^2$. Fig. 3d shows effects of different flow rates on pressure drop of studied UTC filled with nanofluid. As it is seen in this figure, the pressure drop always increases by increasing of flow rate. The value of pressure drop at flow rate of 24 mL/s is about 78 mbar. Fig. 3e shows effects of different solar index ($(T_m-T_{amb})/I$) on energy efficiency of studied UTC filled with nanofluid. As it is seen in this figure, the energy efficiency always reduces by increasing of solar index. The value of energy efficiency at solar index of 1 mK/kW is about 72.12%. Fig. 3f shows effects of different time hours on exergy efficiency of studied UTC filled with nanofluid. As it is seen in this figure, the exergy efficiency of studied UTC at 14:00 has the maximum exergy efficiency among all studied times and about 71.54%. Fig. 3g shows effects of different operating temperature on received energy of studied UTC filled with nanofluid. As it is seen in this figure, the received energy always reduces by increasing of operating temperature. The value of received energy at operating temperature of 23°C is about 0.347 kW/m$^2$.

**Table 5**
Energy and exergy efficiencies for UTC filled with nanofluid

| Time | $I_T$ (W/m$^2$) | $U_L$ (W/m$^2$·K) | $T_{pm}$ (°C) | $T_{out}$ (°C) | $\eta$ (%) | $\psi$ (%) |
|---|---|---|---|---|---|---|
| 09:00 | 560 | 7.51 | 49.43 | 55.89 | 67.24 | 6.66 |
| 09:30 | 630 | 7.57 | 50.42 | 56.95 | 71.22 | 7.22 |
| 10:00 | 750 | 7.43 | 52.78 | 58.29 | 71.59 | 8.16 |
| 10:30 | 830 | 7.61 | 53.90 | 60.36 | 79.78 | 8.76 |
| 11:00 | 925 | 7.69 | 55.87 | 62.59 | 78.06 | 9.15 |
| 11:30 | 992 | 7.72 | 58.80 | 65.40 | 80.26 | 9.67 |
| 12:00 | 1006 | 7.71 | 60.19 | 66.90 | 77.99 | 10.48 |
| 12:30 | 1020 | 7.89 | 61.05 | 67.62 | 77.50 | 9.19 |
| 13:00 | 978 | 7.94 | 62.29 | 69.16 | 77.47 | 9.05 |
| 13:30 | 914 | 7.67 | 62.50 | 69.31 | 76.42 | 9.38 |
| 14:00 | 834 | 7.98 | 65.24 | 72.26 | 72.60 | 9.31 |
| 14:30 | 780 | 7.75 | 65.54 | 72.44 | 72.53 | 9.25 |
| 15:00 | 734 | 7.97 | 65.77 | 72.57 | 69.91 | 8.94 |
| 15:30 | 626 | 8.05 | 66.16 | 72.71 | 69.13 | 8.41 |
| 16:00 | 607 | 8.07 | 67.33 | 72.81 | 68.91 | 8.27 |

Fig. 4 illustrates effects of different nanoparticles diameters on thermal-hydraulic performances of studied UTC. Fig. 4a illustrates effects of different nanoparticles diameters on averaged Nusselt number ratio versus

different volume fractions in studied UTC filled with nanofluid. As it is seen in this figure, nanofluid with nanoparticle diameter of 40nm has maximum values of Nusselt number ratios during all studied volume fractions and is followed by 35nm, 30nm and 25nm cases, respectively. Fig. 4b illustrates effects of different nanoparticles diameters on pressure drop ratio versus different volume fractions in studied UTC filled with nanofluid. As it is seen in this figure, nanofluid with nanoparticle diameter of 40nm has maximum values of pressure drop ratios during all studied volume fractions and is followed by 35nm, 30nm and 25nm cases, respectively. Fig. 4c illustrates effects of different nanoparticles diameters on friction factor ratio versus different volume fractions in studied UTC filled with nanofluid. As it is seen in this figure, nanofluid with nanoparticle diameter of 40nm has maximum values of friction factor ratios during all studied volume fractions and is followed by 35nm, 30nm and 25nm cases, respectively. Fig. 4d illustrates effects of different nanoparticles diameters on PEC ratio versus different volume fractions in studied UTC filled with nanofluid. Higher nanoparticles volume fraction leads to higher thermal conductivity and higher dynamic viscosity. This leads to higher heat transfer rate and pressure drop. Therefore there is a compromise point, where the highest PEC value is achieved. Also higher nanoparticles diameters lead to higher thermal conductivity and higher dynamic viscosity. This leads to higher heat transfer rate and pressure drop. Therefore, there is a compromise point, where the highest PEC value is achieved. As it is seen in this figure, nanofluid with nanoparticle diameter of 40nm has maximum values of PEC ratios during all studied volume fractions and is followed by 35nm, 25nm and 30nm cases, respectively. Also it is seen that for all thermal-hydraulic parameters the ratios always increases by increasing of volume fraction.

Therefore, nanofluid with volume fraction of 4% and nanoparticle diameter of 40 introduced as the best nanofluid in present study. In this figure, for a model with a diameter of 25nm, the value of PEC index, unlike other models, first decreases and then increases. The reason for this lies in its previous diagrams. As can be seen, for a model with a diameter of 25nm, the amount of pressure drop in the volume fraction 2% is very high and the amount of Nusselt number is low.

Therefore, the increase in pressure drop overcomes the improvement of heat transfer and the amount of PEC index decreases at volume fraction 2%. But the most important reason can be considered the low rate of improvement of heat transfer in the conditions of using nanoparticles with a diameter of 25nm.

Fig. 5 presents effects of different tube diameters on thermal-hydraulic performances of studied UTC. Fig. 5a illustrates effects of different tubes diameters on averaged Nusselt number versus different Reynolds numbers in studied UTC filled with nanofluid. As it is seen in this figure, nanofluid with tube diameter of 12nm has maximum values of Nusselt number during all studied Reynolds numbers and is followed by 8nm and 4nm cases, respectively. Also it is realized that averaged Nusselt number values always increase by increasing of Reynolds numbers. Fig. 5b illustrates effects of different tubes diameters on pressure drop versus different Reynolds numbers in studied UTC filled with nanofluid. As it is seen in this figure, nanofluid with tube diameter of 12nm has maximum values of pressure drop during all studied Reynolds numbers and is followed by 8nm and 4nm cases, respectively. Also it is realized that pressure drop values always increase by increasing of Reynolds numbers. Fig. 5c illustrates effects of different tubes diameters on friction factor versus different Reynolds numbers in studied UTC filled with nanofluid.

As it is seen in this figure, nanofluid with tube diameter of 12nm has maximum values of friction factor during all studied Reynolds numbers and is followed by 8nm and 4nm cases, respectively. Also it is realized that friction factor values always reduce by increasing of Reynolds numbers.

Fig. 5d illustrates effects of different tubes diameters on PEC versus different Reynolds numbers in studied UTC filled with nanofluid. As it is seen in this figure, nanofluid with tube diameter of 8nm has maximum values of PEC during all studied Reynolds numbers and is followed by 4nm and 12nm cases, respectively. Also it is realized that PEC values always reduce by increasing of Reynolds numbers.

Therefore, the UTC with tube diameter of 8nm filled with Cu-water nanofluid with 4% volume fraction and 40nm nanoparticle diameter at Re=2000 is introduced as the best model in present study.

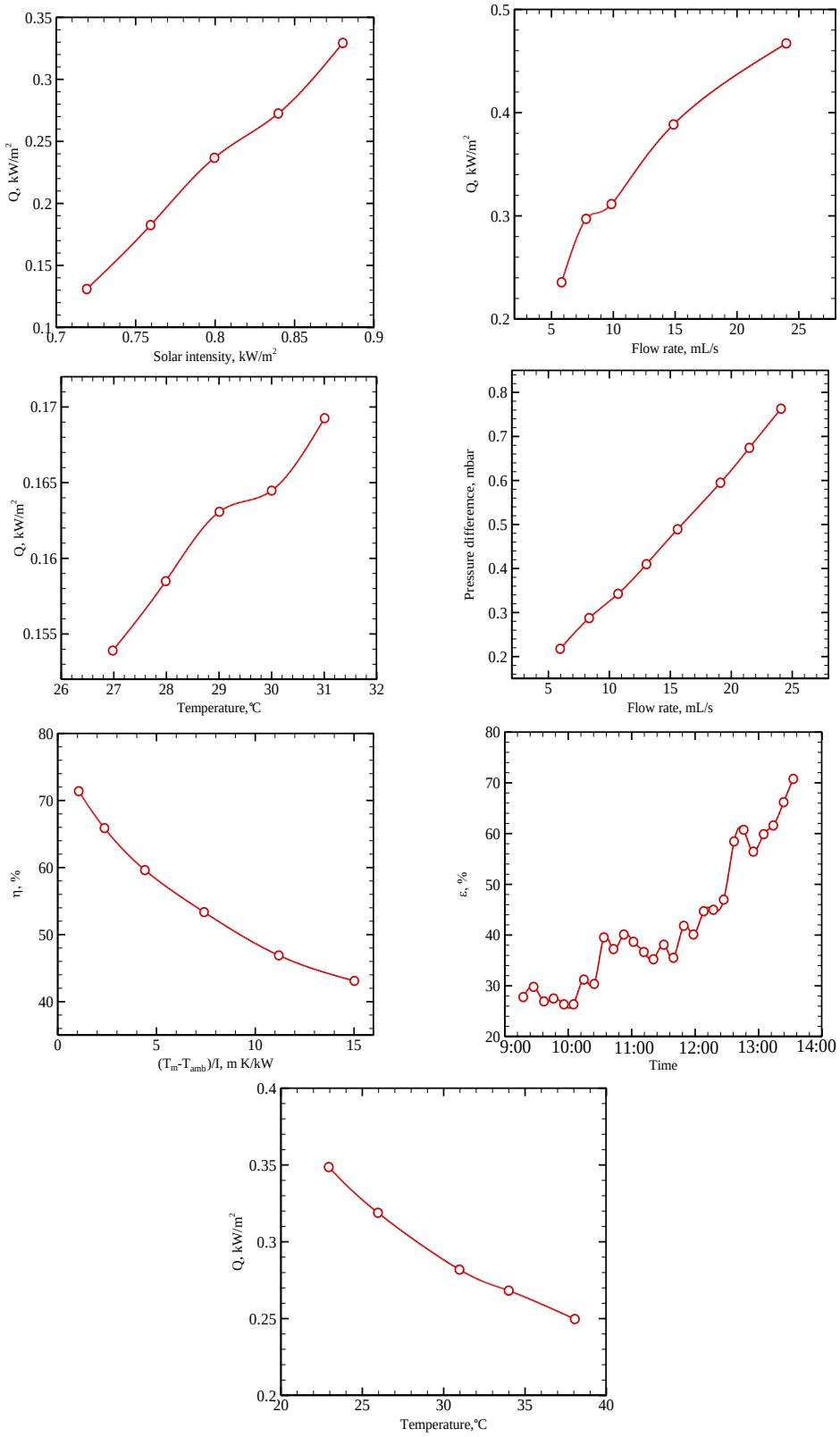


**Fig. 3.** Effects of using nanofluid on different parameters of studied UTC

## CONCLUSION

In this paper, forced convection flow and heat transfer of Cu-water nanofluid in U-Tube collector are studied. The three-dimensional governing equations are numerically solved in the domain by the control volume approach based on the SIMPLE algorithm. Reynolds numbers are considered in laminar-turbulent range of 2000<Re<8000. The most efficient model was achieved by comparison of different parameters to reach the optimal case with the maximum exergy efficiency. According to obtained results, the received energy always increases by increasing of solar intensity. The value of received energy at solar intensity of 0.88 W/m$^2$ is about 0.331 kW/m$^2$. The received energy always increases by increasing of flow rate. The value of received energy at flow rate value of 24 mL/s is about 0.472 kW/m$^2$. Also, the received energy always increases by increasing of inlet flow temperature. The value of received energy at inlet flow temperature of 31°C is about 0.169 kW/m$^2$. The pressure drop always increases by increasing of flow rate. The value of pressure drop at flow rate of 24 mL/s is about 78 mbar. On the other side, the energy efficiency always reduces by increasing of solar index. The value of energy efficiency at solar index of 1 mK/kW is about 72.12%. Besides, the exergy efficiency of studied UTC at 14:00 has the maximum exergy efficiency among all studied times and about 71.54%. The nanofluid flow has higher thermal conductivity than the base fluid and can absorb more solar irradiances. But the nanofluid has also more dynamic viscosity than base fluid which increases the pressure drop penalty and friction factor in system. Higher nanoparticles volume fraction leads to higher thermal conductivity and higher dynamic viscosity. This leads to higher heat transfer rate and pressure drop. Therefore there is a compromise point, where the highest PEC value is achieved. Furthermore, the received energy always reduces by increasing of operating temperature. The value of received energy at operating temperature of 23°C is about 0.347 kW/m$^2$. Nanofluid with nanoparticle diameter of 40nm has maximum values of PEC ratios during all studied volume fractions and is followed by 35nm, 25nm and 30nm cases, respectively.

Nanofluid with tube diameter of 8nm has maximum values of PEC during all studied Reynolds numbers and is followed by 4nm and 12nm cases, respectively. The UTC with tube diameter of 8nm filled with Cu-water nanofluid with 4% volume fraction and 40nm nanoparticle diameter at Re=2000 is introduced as the best model in present study. Higher nanoparticles diameters lead to higher thermal conductivity and higher dynamic viscosity. This leads to higher heat transfer rate and pressure drop. Therefore there is a compromise point, where the highest PEC value is achieved.

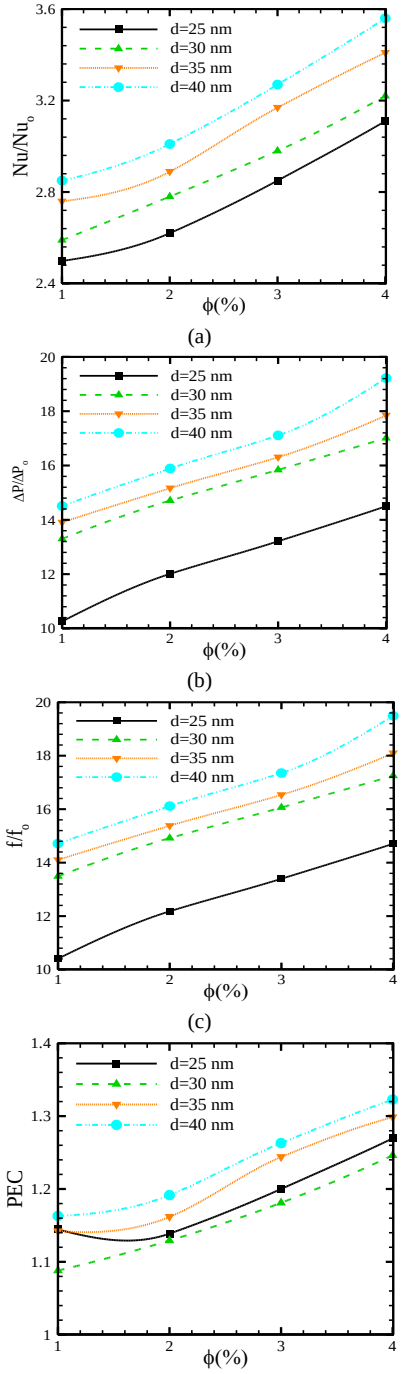


**Fig. 4** Effects of different nanoparticles diameters on thermal-hydraulic performances of studied UTC

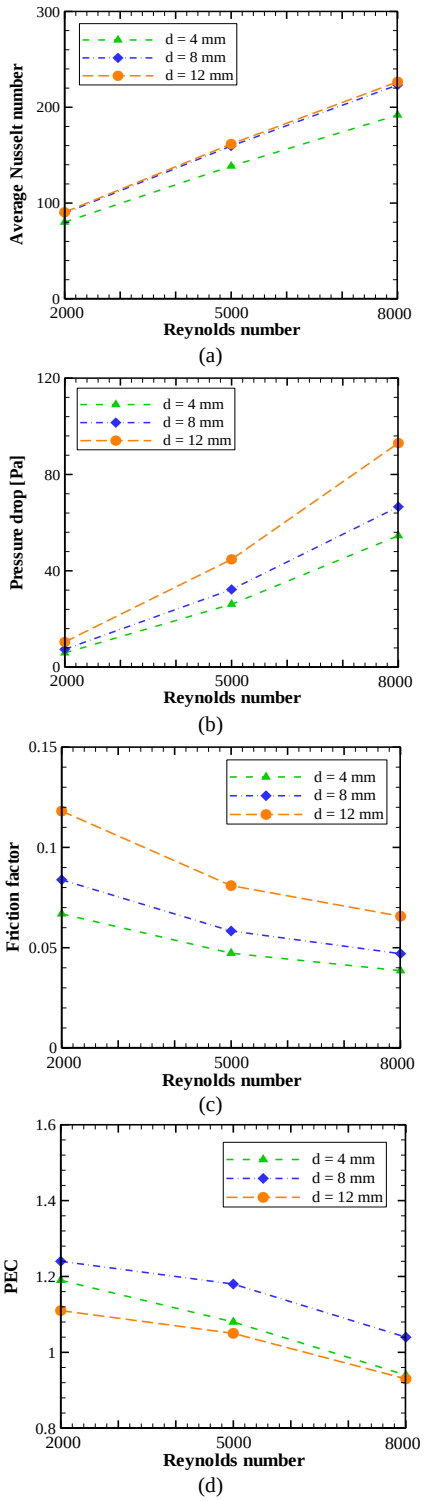


**Fig. 5.** Effects of different tube diameters on thermal-hydraulic performances of studied UTC

## REFERENCES


[1] Kaya H, Arslan K. Nurettin Eltugral, Experimental investigation of thermal performance of an evacuated U-Tube solar collector with ZnO/Etylene glycol-pure water nanofluids, Renewable Energy, Vol. 122, pp. 329-338, **2018**.

[2] Naik BK, Muthukumar P. Performance assessment of evacuated U-tube solar collector: a numerical study, Sādhanā, Vol. 44, No. 23, **2019**.

[3] Kaya H, Arslan K. Numerical investigation of efficiency and economic analysis of an evacuated U-tube solar collector with different nanofluids, Heat Mass Transfer, Vol. 55, No. 581, **2019**.

[4] Sadeghi G, Safarzadeh H, Ameri M. Experimental and numerical investigations on performance of evacuated tube solar collectors, applying synthesized $Cu_2O$/distilled water nanofluid, Energy for Sustainable Development, Vol. 48, pp. 88-106, **2019**.

[5] Wang Q, Yang H, Huang X, Li J, Pei G. Numerical investigation and experimental validation of the impacts of an inner radiation shield on solar receivers, Applied Thermal Engineering, Vol. 132, pp. 381-392, **2018**.

[6] Yang H, Wang Q, Huang X, Li J, Pei G. Performance study and comparative analysis of traditional and double-selective-coated solar receivers, *Energy*, Vol. 145, pp. 206-216, **2018**.

[7] Naphon P, Kornkumjayrit K. Numerical analysis on the fluid flow and heat transfer in the channel with V-shaped wavy lower plate, International Communications in Heat and Mass Transfer, Vol. 35, No. 7, pp. 839–843, **2018**.

[8] Naphon P. Effect of wavy plate geometry configurations on the temperature and flow distributions, International Communications in Heat and Mass Transfer, Vol. 36, No. 9, pp. 942–946, **2009**.

[9] Assato M, Lemos MJ. Turbulence structure and heat transfer in a sudden expansion with a porous insert using linear and non-linear turbulence models, International Journal of Thermal Science, Vol. 141, pp. 1–13, **2019**.

[10] Sui Y, Teo CJ, Lee PS, Chew Y, Shu C. CFD Analysis of microchannel heat sink in taper shaped manifold arrangements, 2019 5th International Conference on Advanced Computing & Communication Systems, 10.1109/ICACCS.2019.8728345, **2019**.

[11] Duan Z, Muzychka YS. Pressure Drop of Microchannel Plate Fin Heat Sinks, Micro mechanics, Vol. 10, No. 2, **2019**.

[12] Zhang L, Che D. Influence of corrugation profile on the thermal hydraulic performance of cross-corrugated plates, Numerical Heat Transfer, Part A: Applications, Vol. 59, No. 4, pp. 267–296, **2011**.

[13] Zhang L, Che D. Turbulence models for fluid flow and heat transfer between cross-corrugated plates, Numerical Heat Transfer, Part A: Applications, Vol. 60, No. 5, pp. 410–440, **2011**.

[14] Ronnelid M, Karlsson B. The use of corrugated booster reflectors for solar collector fields, Sol. Energy 65 (6) 343–351, **1999**.

[15] Tanaka H. Solar thermal collector augmented by flat plate booster reflector: Optimum inclination of collector and reflector, Appl. Energy 88, 1395–1404, **2011**.

[16] Monowe P, Masale M, Nijegorodov N, Vasilenko V. A portable single-basin solar still with an external reflecting booster and an outside condenser, Desalination 280 332–338, **2011**.

[17] Ljiljana T, Zoran T. Pavlovic, Optimal position of flat plate reflectors of solar thermal collector, Energy, Build 45, 161–168, **2012**.

[18] T. Zoran. and T. Ljiljana., Variation of reflected radiation from all reflectors of a flat plate solar collector during a year, Energy 80, 75-84, **2015**.

[19] Tanaka H. Theoretical analysis of solar thermal collector and flat plate bottom reflector with a gap between them, Energy Reports 1, 80–88, **2015**.

[20] Kiran Naik B, Bhowmik M, Muthukumar P. Experimental investigation and numerical modelling on the performance assessments of evacuated U – Tube solar collector systems, Renewable Energy, Vol. 134, pp. 1344-1361, **2019**.

[21] Sharafeldin MA, Gróf G, Abu-Nada E, Mahian O. Evacuated tube solar collector performance using copper nanofluid: Energy and environmental analysis, Applied Thermal Engineering, 114205, http://doi.org/10.1016/j.applthermaleng.2019. 114205. 2019

[22] Sharafeldin MA, Gróf G. Efficiency of evacuated tube solar collector using WO3/Water nanofluid, Renewable Energy, Vol. 134, pp. 453-460, https://doi.org/10.1016/j.renene.2018.11.010, **2019**.

[23] Sarafraz MM, Safaei MR. Diurnal thermal evaluation of an evacuated tube solar collector (ETSC) charged with graphene nanoplatelets-methanol nano-suspension, Renewable Energy, Vol. 142, 2019, pp. 364-372, https://doi.org/10.1016/j.renene.2019.04.091, **2019**.

[24] Roja A, Gireesha BJ, Prasannakumara BC. MHD micropolar nanofluid flow through an inclined channel with entropy generation subjected to radiative heat flux, viscous dissipation and multiple slip effects, Multidiscipline Modeling in Materials and Structures, Vol. 16 No. 6, pp. 1475-1496, **2020**.

[25] Prasannakumara BJ, Gireesha BC, Gorla SR, Krishnamurthy MR. Effects of Chemical Reaction and Nonlinear Thermal Radiation on Williamson Nanofluid Slip Flow over a Stretching Sheet Embedded in a Porous Medium, Journal of Aerospace Engineering, Vol. 29, No. 5, 04016019, 2016.

[26] Gireesha BJ, Umeshaiah M, Prasannakumara BC, Shashikumar NS, Archana M. Impact of nonlinear thermal radiation on magnetohydrodynamic three dimensional boundary layer flow of Jeffrey nanofluid over a nonlinearly permeable stretching sheet, Physica A: Statistical Mechanics and its Applications, Volume 549, 124051, 2020.

[27] Abeer Baslem G, Sowmya BJ, Gireesha Prasannakumara BC, Rahimi-Gorji M, Minh Hoang N. Analysis of thermal behavior of a porous fin fully wetted with nanofluids: convection and radiation, Journal of Molecular Liquids, Volume 307, 112920, 2020.

[28] Sowmya G, Gireesha BJ, Sindhu S. Investigation of Ti6Al4V and AA7075 alloy embedded nanofluid flow over longitudinal porous fin in the presence of internal heat generation and convective condition, Communications in Theoretical Physics, Vol. 72, 025004, 2020.

[29] Sabziparvar AA. General formula for estimation of monthlymean global solar radiation in different climates on the south and north coasts of Iran, International Journal of Photoenergy, Vol. 2007, 94786, 1–7, **2017**.

[30] Abbasian–Arani AA, Sadripour S, Kermani S. Nanoparticle shape effects on thermal-hydraulic performance of boehmite alumina nanofluids in a sinusoidal–wavy mini-channel with phase shift and variable wavelength, International Journal of Mechanical Sciences, Vol. 128–129, 550–563, **2017**.

[31] Sadripour S. First and second laws analysis and optimization of a solar absorber; using insulator mixers and MWCNTs nanoparticles, Global Journal of Researches in Engineering A: Mechanical and Mechanics, Vol. 17, No. 5, 37–48, **2017**.

[32] Sadripour S, Adibi M, Sheikhzadeh GA. Two different viewpoints about using aerosol-carbon nanofluid in corrugated solar collectors: Thermal-hydraulic performance and heating performance, Global Journal of Researches in Engineering A: Mechanical and Mechanics, Vol. 17, No. 5, 19–36, **2017**.

[33] Daffie JA, Beckman WA. Solar engineering of thermal progress, 4th ed. John Wiley & Sons, **2009**.

[34] Sadripour S. 3D Numerical Analysis of Atmospheric-Aerosol/Carbon-Black Nanofluid Flow within a Solar Air Heater Located in Shiraz, Iran, International Journal of Numerical Methods for Heat and Fluid Flow, Vol. 29, No. 4, pp. 1378-1402, **2019**.

[35] Sadripour S, Chamkha AJ. The Effect of Nanoparticle Morphology on Heat Transfer and Entropy Generation of Supported Nanofluids in a Heat Sink Solar Collector, Thermal Science and Engineering Progress, Vol. 9, pp. 266–280, **2019**.

[36] Baccoli R, Mastino CC, Innamorati R, Serra L, Curreli S, Ghiani E, Ricciu R, Marini M. A mathematical model of a solar collector augmented by a flat plate above reflector Optimum inclination of collector and reflector, Energy Proc. 81, 205-214, **2015**.

[37] Behrooz M, Palideh V, Mokhtari F. Performance improvement of the finned passive PVT system using reflectors like removable insulation cover, Appl. Therm. Eng. 94, 341–349, **2016**.

[38] Dutta Gupta KK, Saha S. Energy Analysis of Solar Thermal Collectors, Renewable energy and environment, Vol. 33, No. 1, pp. 283-287, **1990**.